MDPI

Article

Macroscopic and Petrographic Analyses of the Mortars from the Roman *villa* of Noheda (Villar de Domingo García, Cuenca)

Miguel Ángel Valero Tévar [1,*], Xoan Moreno Paredes [2,*], Pablo Guerra García [3,*], Xabier Arroyo Rey [4,*] and Nelia Valverde Gascueña [5,*]

1 Facultad de Ciencias de la Educación y Humanidades de Cuenca, Universidad de Castilla-La Mancha, Avda, de Los Alfares 44, 16071 Cuenca, Spain
2 Museo Geominero (IGME-CSIC), Calle de Ríos Rosas, 23, 28003 Madrid, Spain
3 Centro Asociado UNED Cuenca, Universidad Nacional de Educación a Distancia, Calle Colón, 6, 16002 Cuenca, Spain
4 CAI de Ciencias de la Tierra y Arqueometría, Unidad de Técnicas Geológicas, Universidad Complutense de Madrid, Calle de José Antonio Novais, 12, 28040 Madrid, Spain
5 Escuela Politécnica de Cuenca, Campus Universitario, Universidad de Castilla-La Mancha, 16071 Cuenca, Spain
* Correspondence: miguelangel.valero@uclm.es (M.Á.V.T.); x.moreno@igme.es (X.M.P.); pabguerra@cuenca.uned.es (P.G.G.); xarroyo@ucm.es (X.A.R.); nelia.valverde@uclm.es (N.V.G.)

Abstract: The Roman *villa* of Noheda, located in the municipality of Villar de Domingo García (Cuenca), is one of the most important archaeological sites in Spain and one of the most important museum complexes in Europe. In recent years, several archaeological investigations have been developed (archaeometry of building materials, natural resources, ways and roads). Furthermore, various restoration and consolidation works have been carried out on structures, walls and floors. The archaeological management team requested a characterisation of the mortars found in the coatings of the walls and floors of the complex to identify differences in its production. After checking the rooms, the state of conservation of the elements and the significance of the materials used, several mortar samples were analysed by means of macroscopic techniques before applying a petrographic analysis. The results showed an interesting variety in the distribution of aggregates, a complex microstratigraphy and a range of grain sizes in the mortars from different rooms. Magnesium, silica and aluminium from limestone were found. Crushed and powdered limestone was used as an aggregate with irregular distribution. Calcite nodules were observed as evidence that the mortar had been poorly mixed in preparation.

Keywords: Roman *villa*; late antiquity; mortar; Petrography; archaeometry

1. Introduction

There are written references to the Roman *villa* of Noheda dating back to ancient times [1–5]. The site is located in the centre of the Iberian Peninsula, about 18 kilometres north of the city of Cuenca. It lies a mere 500 metres northeast of the village it is named after and is part of the municipality of Villar de Domingo García (Figure 1).

In 2012, it was declared a "Heritage of Cultural Interest", mainly because of the mosaics discovered there [6,7]. The most prominent evidence of site occupation is from late antiquity, although evidence has been documented from other eras. Research done in the past few years has confirmed the existence of archaeological structures under the late imperial Roman *villa*, which can be dated to the 1st century A.D. Due to the limited surface area excavated to date, they cannot yet be properly interpreted. There are also archaeological remains that indicate habitation in the Iron Age. In addition, the territorial analyses of the immediate surrounding area indicate intense human activity in these regions [8], providing evidence of the uninterrupted presence of a settlement from the prehistoric era until the Early Middle Ages.

Despite this lengthy human occupation of the site, the late Roman period is the most notable, marked by an intense occupation phase, as well as particularly noteworthy constructions. A whole new building complex was constructed, with new structures of a considerable size (Figure 2). In turn, these were subsequently expanded or altered in order to monumentalise the *villa*. Chronologically, this phase coincides with the proliferation of the great *villae* documented in the Western half of the Empire [9–15].

Thus far, only two areas have been excavated from this phase: one of the sectors of the *pars urbana*, which is analysed below, and structures from the pars rustica. The presence of the latter indicates that the complex was endowed with all the buildings needed for agricultural activity, which was inherent to the concept of the rustic *villa* [16–21].

Concerning the pars urbana, it should be noted that our efforts were focused on these areas, excavating the *balneum* and some of the rooms from the residential sector. The thermal bathhouse is nearly 900 m^2 in size, and its layout is axial-symmetric [22], with a number of special rooms arranged around the central axis, a narthex-type entrance, the apodyterium, and the great *frigidarium*. As found in other thermal compounds dated to the end of the 3rd century and throughout the 4th, in Noheda, it is easy to discern linking for increasingly complex designs and a profusion of apses or octagonal structures.
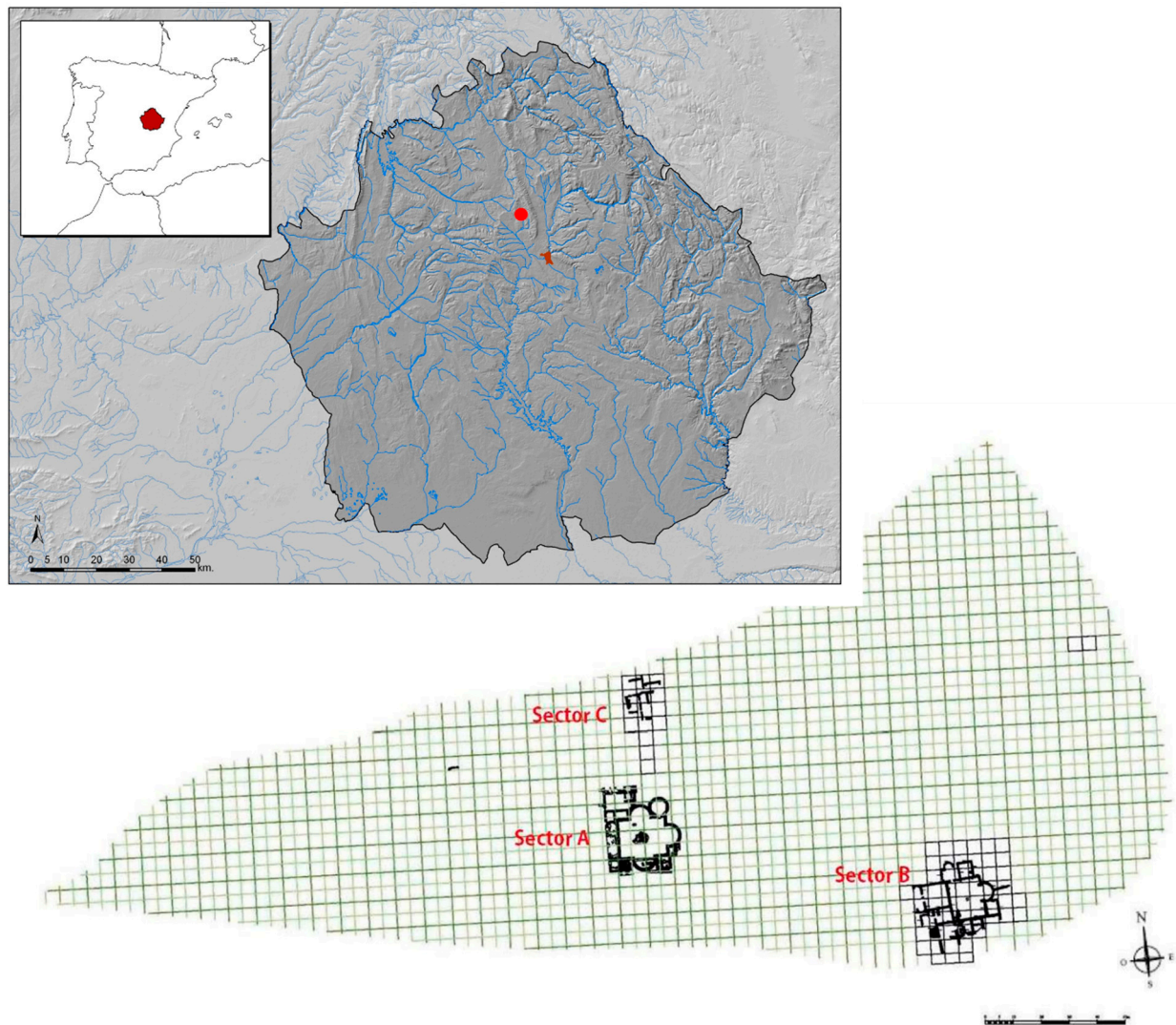

Figure 1. Location of the settlement (red dot) within Cuenca Province, and planimetry of the Roman *villa* of Noheda, indicating the archaeological sectors.

Figure 2. Aerial view of the building constructed at Noheda to protect and exhibit the mosaics. Photo: Antonio Gálvez.

As for the structures intended for residential use, to date, seven rooms have been completely unearthed. Among these, is the Triconch room, which has impressive dimensions (290.64 m^2) and a complex architectural structure. It also has extraordinary flooring and carefully decorated walls, with a skirting board made of marble tiles along the bottom and a wall painting above. Given its quadrangular shape with exedras on three of the sides, it can be classified as an example of the type of three-apsed (triconch) rooms that were frequently built in the most luxurious residential complexes dating from the end of the 3rd century A.D. on [23]. These rooms have a trichora structure and can be interpreted as triclinia [24–27]. As such, they reflect the alignment of the architectural form with the new trends in spatial organisation for banquet guests, with couches arranged in a semicircle, the *stibadia* [28,29].

It is in this room that we find an exceptional mosaic floor with a conserved area of 231.62 m^2, mostly made of *opus vermiculatum* in a wide variety of colours (Figure 3). Coloured glass paste is used to create many different tones, including gold. The mosaic is rectangular, with a wide central area divided into six figurative panels depicting scenes of a mythological and allegorical nature, featuring more than 160 figures mingling to create scenic ensembles. Then, there is the frame, edged with spirals of acanthus leaves, and lastly, the geometric decorations in the three exedras [30,31].

What is notable about this piece is the meticulous technical and stylistic features, its elaborate execution, its great artistic quality, its iconographic richness, and its complex composition. All this, together with its magnificent dimensions and its good state of conservation, make it exceptional, a unicum.

During the 2020 season, the archaeological management team requested the characterisation of some of the mortars documented in the archaeological site. The mortar samples were found in both the original walls and slabs recovered from the different stratigraphic layers precisely identified in time and place. They mostly corresponded to wall coatings and were well-compacted and in good condition. Both the sampling process and the subsequent analyses were carried out in collaboration with the archaeological management team.

Figure 3. Detail of the embrace between Pelops and Hippodamia. Photo: Miguel Ángel Valero.

This study combines two commonly used characterisation methods: reflected light macroscopy and polarised optical microscopy. The first stage was carried out using magnifying glasses and stereomicroscopes after first preparing the samples by cutting them and polishing the surfaces to ensure the correct visualisation. Based on the results obtained, the samples showing the most relevant data were subject to a thorough petrographic analysis of the corresponding thin sections.

2. Samples and Sampling Points

Most of the mortars analysed come from stratigraphic layers of deposits documented in the archaeological excavation phases. As can be seen in the table below (Table 1), the acronym used was NO, followed by a number. Samples NO2–NO5 come from samples collected from interior rooms, while samples NO1, NO6, and NO7 come directly from the preserved wall facings. None of the samples weighed more than 100 g, and on average, they were only 5 cm^2. The entire sampling phase followed standardised procedures described in reviewed publications [32]. The samples obtained by direct extraction were first analysed by means of macroscopy in situ in order to identify the samples for microstratigraphic analysis. The samples were carefully extracted using a scalpel and a laboratory spatula. Consistent and compacted samples were collected from all the original construction layers from the pictorial layer to the rendering base.

None of the samples weighed more than 100 g, and on average, they were only 5 cm^2. The entire sampling phase followed standardised procedures described in reviewed publications [32]. The samples obtained by direct extraction were first analysed by means of macroscopy in situ in order to identify the samples for microstratigraphic analysis. The samples were carefully extracted using a scalpel and a laboratory spatula. Consistent and compacted samples were collected from all the original construction layers from the pictorial layer to the rendering base.

Table 1. Distribution of the samples, provenance, and types.

Num.	Location	Place	Type
NO1	North Exedra	-	Mortar slab with painting of frescoes
NO2	Pit 1	UE 3	Subsample 1: Plastered mortar board with decorative incisions
			Subsample 2: Mortar board with painting of frescoes
NO3	Pit 9	UE 21	Mortar slab with simple coating
NO4	Pit 13	UE 9	Mortar slab coating with decorative incisions
NO5	Pit 21	UE 2	Mosaic slab with tessellate and bedding mortar
NO6	Room C West Side of South Exedra	Skirting	Mortar slab with plain coating
NO7	Room I West Side of North Exedra	Wall painting	Mortar slab with painted coating

3. Methodology

The samples were analysed using NIHRM techniques (Non-Invasive High-Resolution Macroscopy) with high-power lenses to capture images and apply colorimetric analysis [33]. Several studies have been carried out using this method [34,35], which yields data relating to the components of a material, and their distribution, morphology, etc. Through the use of these techniques, the basic components of the aggregates and binders were identified, and the different construction or microstratigraphic phases of the mortars, as well as the grain sizes of the aggregates identified, their distribution, and their sphericity index, etc. The data were obtained from macrophotographs taken by optical instruments, and these images were later processed through different optical and colour analysis programs. The tools and software used are described below, and the methods are supported by previous literature [36].

Data related to grain size, microstratigraphy, and basic morphology were obtained through the optical software programs JMicrovision and ImageJ [37,38]. Regarding the granulometric study, a statistical calculation must be performed based on hyperspectral analysis. Using this method, it is also possible to calculate surface areas in a microscopic image, analysing the space occupied by a colour or the different ranges that compose said colour, indicating the lime matrix of a mortar or the ceramic in the aggregates, for example. Three-dimensional scans of the surface and thermal analyses were carried out using ImageJ software.

Regarding the morphological study, based on different tests carried out by other research groups, some criteria were agreed for the classification of the components that make up the mortars, depending on the distribution and morphology of the aggregates. One of these criteria was the Raymond-Powder Classification, which was used to determine the type of aggregate employed based on the shape (sphericity). The use of these classification criteria is combined with image processing techniques, primarily at the macro level. There are many studies that support the use of this procedure, which has been used to develop pathology identification protocols, quantitative analysis techniques, etc. [39–43].

Having obtained the results of the macroscopic analysis, NO1 and NO2 were selected based on the quality and relevance of the samples and analysed using polarised optical microscopy to determine their mineralogical characteristics. To that end, two petrographic thin sections were prepared and inspected.

The technical instruments used in the macroscopy stage were: a Marés Carton stereomicroscope with double light source and 50–400× magnification; a Veho USB endoscope, model VMS-004, 20–400× magnification, 8 LED lights, and a micrometric lens calibrated with a 1-mm micrometre attached and a Bresser digital microscope with a 5-MP CMOS sensor and 40–1400× magnification. The data obtained were processed using programs such as VehoCapture 1.3, Gimp 2.8, JMicrovision 1.2.7, and Micam 1.6, specifically designed

for the treatment of macro and microscopic images, as well as ImageJ 1.8 programs and FiJi for vector calculations, 3D viewing, and chromatic and thermal analyses.

Regarding the microscopic characterisation, a ZEISS Primotech microscope was used for petrographic analysis, together with the Matscope digital application. The microscopic study yielded information on the mineralogy and texture of the mortar samples.

4. Results

4.1. Macroscopy

The macroscopic analysis of the composition of the mortars suggests a lime-based binder and silico-calcareous aggregates of fine-medium size. Regarding the granulometry, with the exception of sample NO6, which had aggregates with an average diametre of above 3 mm (and can therefore be classified as concrete type), the mortars are mainly intended for use in finishing coats and plasters.

Looking at the distribution of the aggregates and the coefficient of sphericity, it can be said that the mortars present a balanced distribution of aggregates in the matrix, with an evident presence of sand particles (clean, without any interior fractures but angled perimetre). The mixtures with fine or very fine aggregates, present in the layers that serve as the pictorial base, are especially interesting. These aggregates are characterised by the almost imperceptible presence of quartz and small particles of mica. This aspect can be seen in samples NO2 (I) and NO5. The results are shown in the table below (Table 2).

Table 2. Granulometry results.

Sample	Binder	Aggregate	Granulometry (Type)	Distribution	Raymond-Class
NO1	Lime	Siliceous and Calcareous	Medium Mortar	Regular Pseudo-isodome	Sub-rounded Sub-angular
NO2 (I)	Lime	Siliceous	Very fine Mortar	Regular Isodome	Sub-rounded Rounded
NO2 (II)	Lime	Siliceous and Calcareous	Medium Mortar	Irregular Pseudo-isodome	Sub-rounded Rounded
NO3	Lime	Siliceous and Calcareous	Fine-medium Mortar	Irregular Pseudo-isodome	Sub-angular Angular
NO4	Lime	Siliceous and Calcareous	Medium Mortar	Regular Pseudo-isodome	Sub-angular Sub-rounded
NO5	Lime	Siliceous and Calcareous	Fine Mortar	Regular Isodome	Sub-rounded Rounded
NO6	Lime	Siliceous and Calcareous	Medium Concrete	Regular Pseudo-isodome	Sub-angular Sub-rounded
NO7	Lime	Siliceous and Calcareous	Fine-medium Mortar	Irregular Pseudo-isodome	Sub-angular Angular

Another relevant outcome of the study is the documentation of the existing microstratigraphy in some samples. The sequence of superimposed layers has been characterised as follows (Table 3):

Table 3. Microstratigraphy of the samples (thickness in mm).

Sample	NO1	NO2	NO3	NO4	NO5	NO6	NO7
Arriccio (first layer)	3–10	2–8	2–4	3–5	-	4–6	3–6
Intonaco (second layer)	0.5–1	0.5–1.5	0.5–1	2–4	-	2–4	1–2
Pictorial	<0.5	<0.5	-	-	-	-	<0.5

The thickness of the arriccio layer given above is not necessarily accurate, since, in the sampling or detachment phase, part of the arriccio remained adhered to the original masonry. The intonaco layers are relatively thin (as shown by the thermal LUT depicted in photo 6 of Figure 4), except for sample NO4, which has a greater maximum/minimum difference and no pictorial layer; something similar can be seen in sample NO6. Conversely, NO1, NO2, and NO3 have similar base layers and no significant variations. No microstratigraphic results were found for sample NO5, as it is a mortar used as an adhesive for the mosaic.
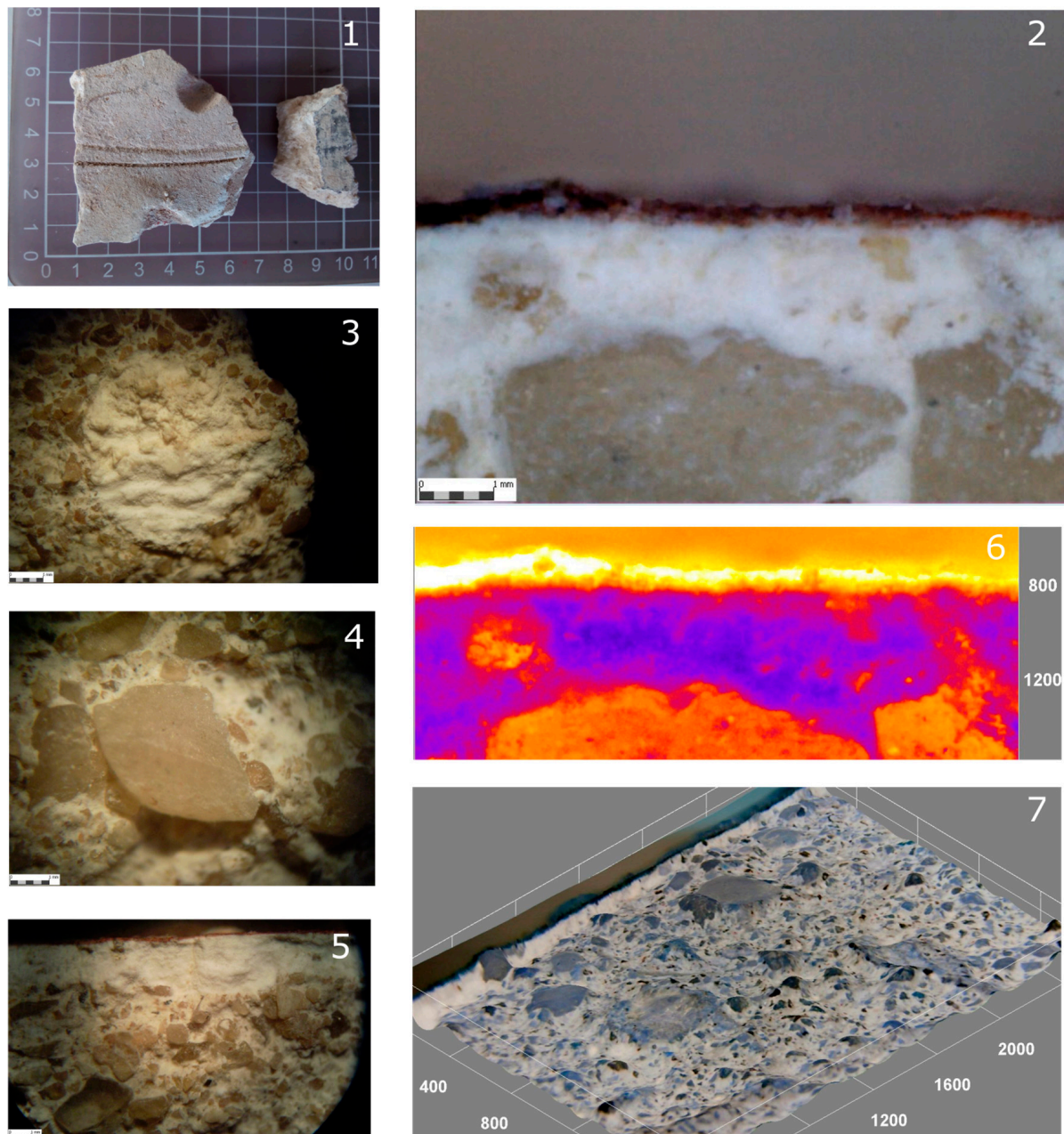
Figure 4. Macroscopic analysis of sample NO1 (1 mm scale): (1) Photo of sample before treatment, (2) cross-section without treatment (×50 mag.), (3) lumps of lime, (4) quartz grains, (5) cross section with reflected light, (6) thermal LUT analysis of cross section using ImageJ software showing the outside layer (yellowish), and (7) photogrammetry surface of sample using ImageJ software showing the irregular distribution and sizes of aggregates.

Regarding the granulometric measurements, the hyperspectral analysis revealed a wide variety of sizes in the aggregates in terms of the area-to-perimeter ratio, as can be seen in Figure 4, photo 7. Table 4 shows an homogeneous coefficient ratio of aggregates. NO1 and NO3 samples present a similar area–perimeter ratio, in relation with the rest, with similar dates (both main examples are referred to in Figure 5). The results obtained are the following:

Table 4. Area-to-perimeter ratio results.

Sample	NO1	NO2	NO3	NO4	NO5	NO6	NO7
Coeff.	0.8888	0.9568	0.8947	0.9236	0.9626	0.9786	0.9159
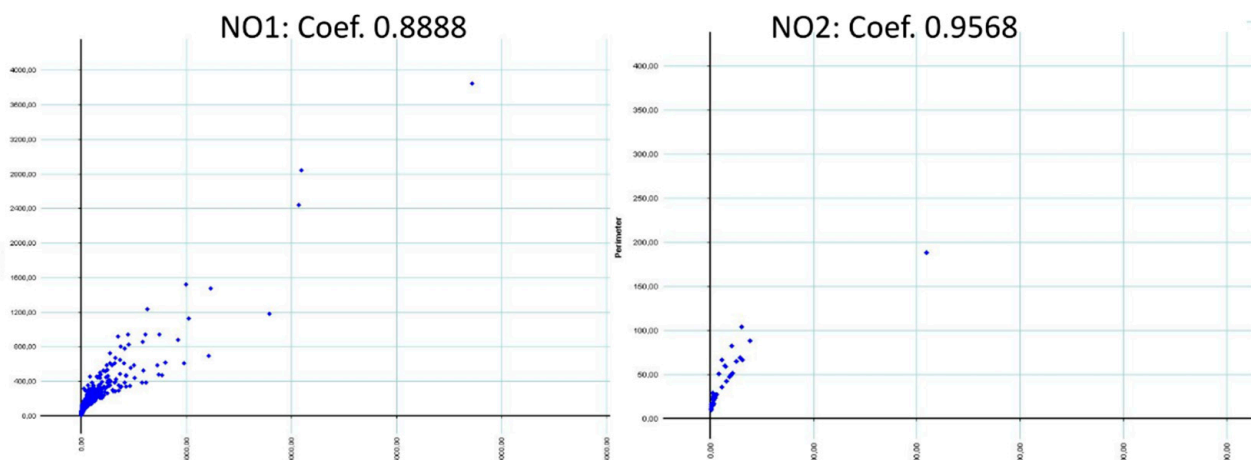
Figure 5. Graphs of the coefficient of sphericity in NO1 and 2, the most relevant results based on the area-to-perimeter ratio (JMicrovision Software). Two groups are found according to the sizes and 2D surfaces.

The data revealed mortars with lime binders and siliceous and calcareous aggregates of different sphericity, distribution, and shape. In general, except for a few specific cases, the mixtures are of very good quality with subangular and subrounded aggregates well-mixed and with a good quality binder. The granulometry of all the samples indicates that they are mortars, except for sample NO6, which is a concrete with abundant aggregates above 3/5 mm. The samples NO2-I and NO5 present aggregates below 1 mm on average. The morphology of the remaining samples corresponds to Roman mortars intended for coatings and plasters with pictorial decorations.

For the most part, the aggregates are siliceous, although there is an identifiable presence of calcareous aggregates, which has been verified by microscopic analysis. The latter are mainly complete or fragmented quartzites in the inert part of the mixtures.

Conversely, the siliceous aggregates are primarily composed of quartz, feldspars, and mica, corresponding to all of the samples. The quartz presents broken textures under the microscope as a result of selective crushing (for better binding). The edges of the grains in these aggregates could improve the binding process, making the mortar much more resistant to mechanical stresses. Therefore, this fact is considered evidence of careful manufacture.

The distribution of the aggregates is sometimes irregular, with clusters forming, as in samples NO4 and NO7. This implies a certain carelessness in production. The aggregates present in the coating layers have a refined appearance with a smaller grain size. No ceramic or pozzolanic aggregates or any hydraulic type of aggregates have been found.

Noteworthy among the components identified are the organic additives found in sample NO5, belonging to the bedding mortar of a mosaic. The localised imprints mostly

belong to plant phytoliths (shown in Figure 6 using microphogrametric analyses conducted with ImageJ software), although it has been possible to identify some remains of microvertebrate fauna. These imprints are assumed to have occurred during the setting and hardening process.
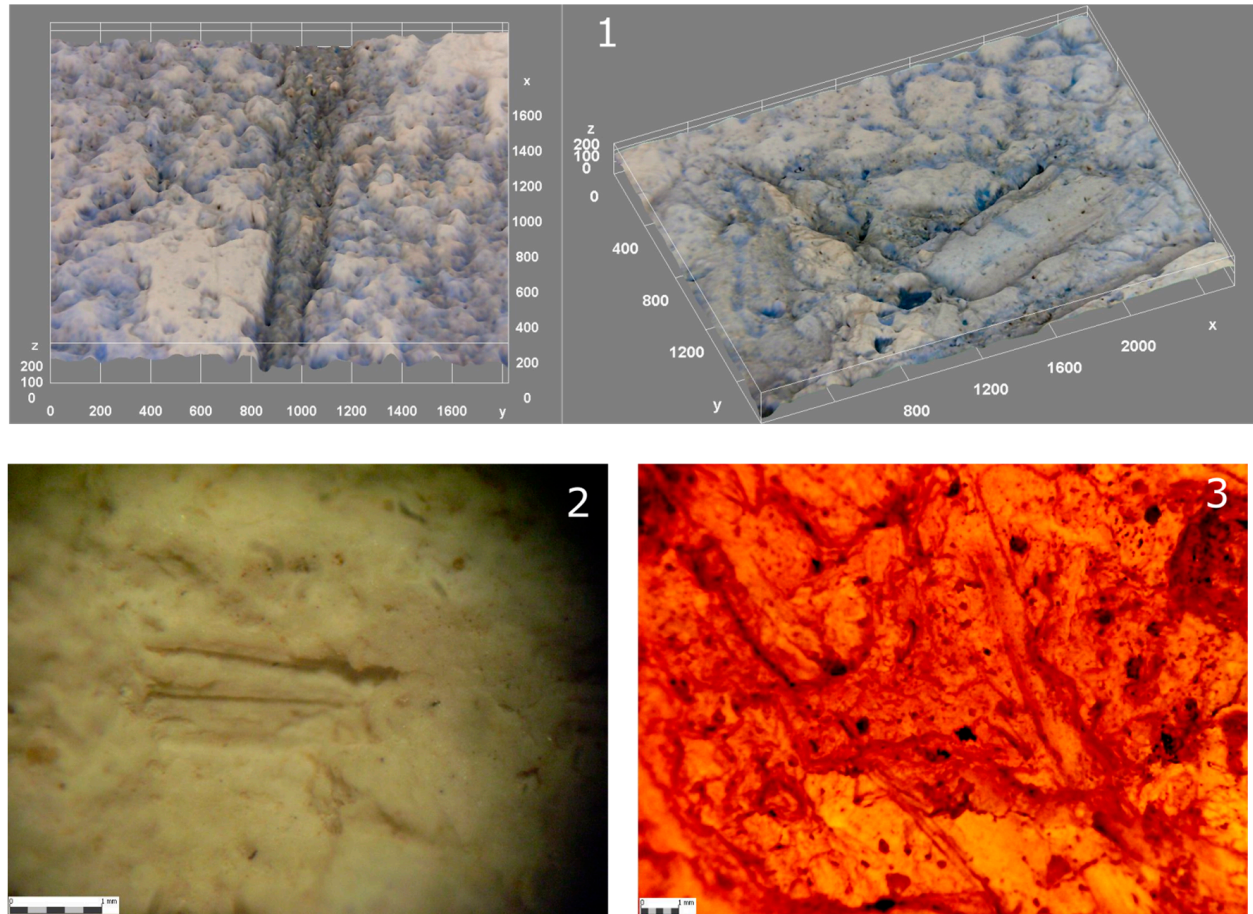

Figure 6. Organic remains in samples NO2 and NO5 (1 mm scale): (1) 3D scan of surface showing fibres (left) and microvertebrates prints (right) in sample NO2, (2) possible dental print in NO5, and (3) infrared picture with several organic prints in sample NO5.

Carbonate nodules are found in all samples, with varying sizes, depending on the mixture. NO1, NO3, and NO6 are the samples with largest nodules. This finding has been corroborated through microscopic analysis, with the documentation of recrystallisations associated with calcite in the NO2 sample.

In terms of microstratigraphy, we find an arriccio showing the morphological characteristics described above, and various intonacos of different thicknesses depending on the presence or absence of a pictorial layer, showing very fine aggregates and high-quality finishes (Figure 7). These finishes can function as base for pictorial decoration (as in samples NO1, NO2-II, and NO 7). Using in-situ microphotographs and colourimetry (pictures taken using portable lenses and processed using Micam, ImageJ, and Gimp software), black, red, and white tones (base backgrounds) with irregular lines and spatula marks on the surface have been identified. These spatula marks are accompanied, in some cases, by outer layers of organic material, as has been verified in the optical microscopy of the NO1 and NO2 samples. This material could be an organic binder applied after the pictorial finish (maybe a casein fraction). The chemical analysis is currently in progress.
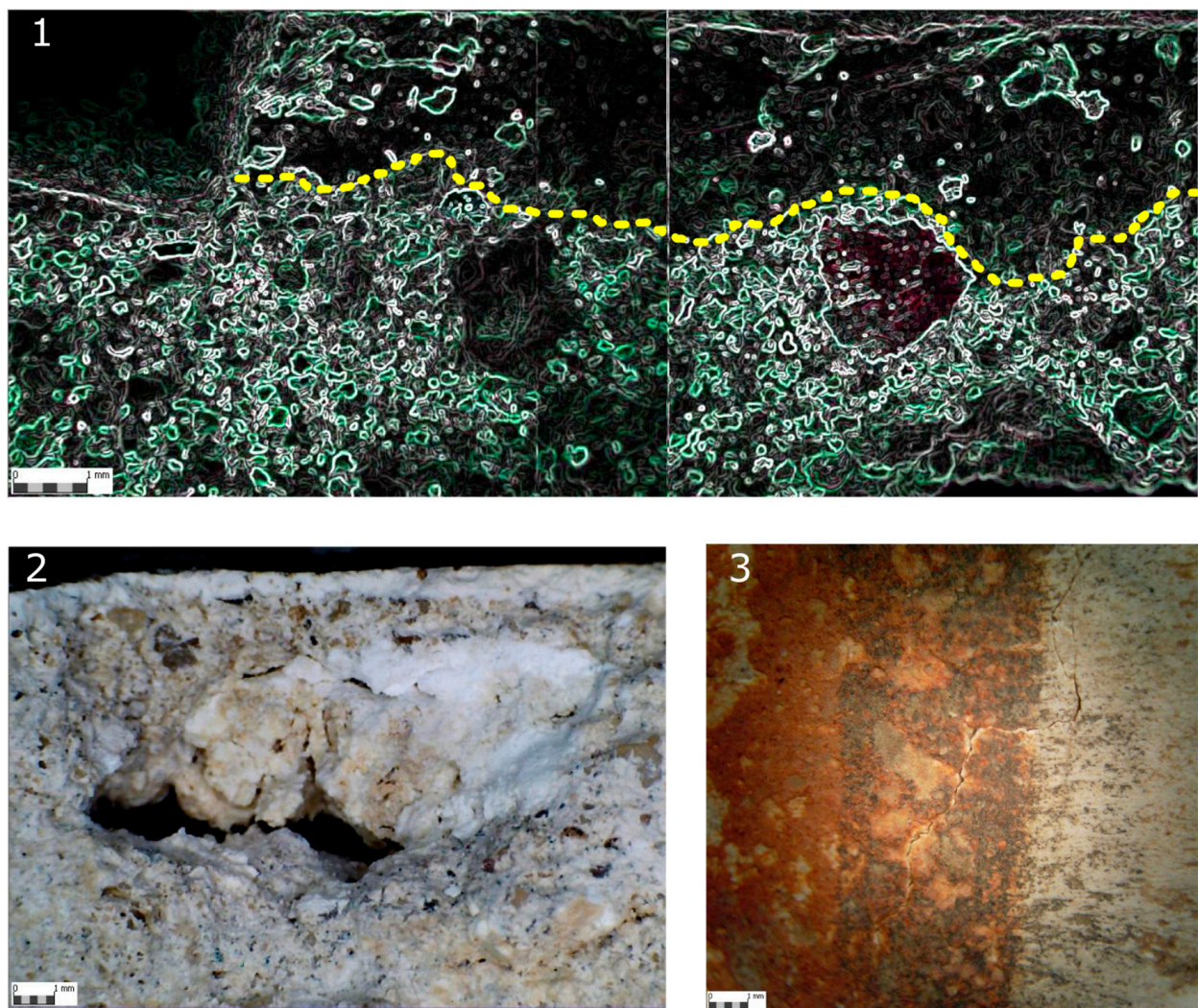
Figure 7. (1) Sobel treatment in sample NO4 showing the difference (separated by yellow dashed line) between the outside layer (less presence of aggregates) and inside (arriccio and intonaco). (2) Sample NO2 with recalcification in the pores (left). (3) Spatula marks on the surface of sample NO7.

4.2. Optical Microscopy

Having completed the macroscopic analysis and reviewed the results, two samples were chosen, mainly due the presence of organic material and their general morphological qualities: NO1 and NO2. Thin sections were created from both, and a polarised optical microscopy was performed, the results of which are described below.

4.2.1. Sample NO1

The NO1 mortar has a homogeneous texture somewhere between granular (aggregates in contact) and floating (aggregates suspended in the binder) with a binder/aggregate ratio of around 2/1. The aggregates are crushed silicate for the most part and present generalised internal fracturing. The grain size ranges from a few microns to approximately 500 microns, covering all grain sizes and thus ensuring the compactness of the mortar.

In turn, the aggregates are very angular, facilitating interlocking (Figure 8A,B). The aggregates are mainly quartz grains (Figures 8E,F and 9C,D), containing, in turn, microcline and plagioclase feldspars (triangular grain in Figure 8E,F), mica, and a low percentage of calcareous rock fragments (central aggregate in Figure 9A,B). In general, opaque minerals are not observed, although occasional reddish aggregates can be seen, which could be iron oxides or altered mica (reddish grains in Figure 8A).
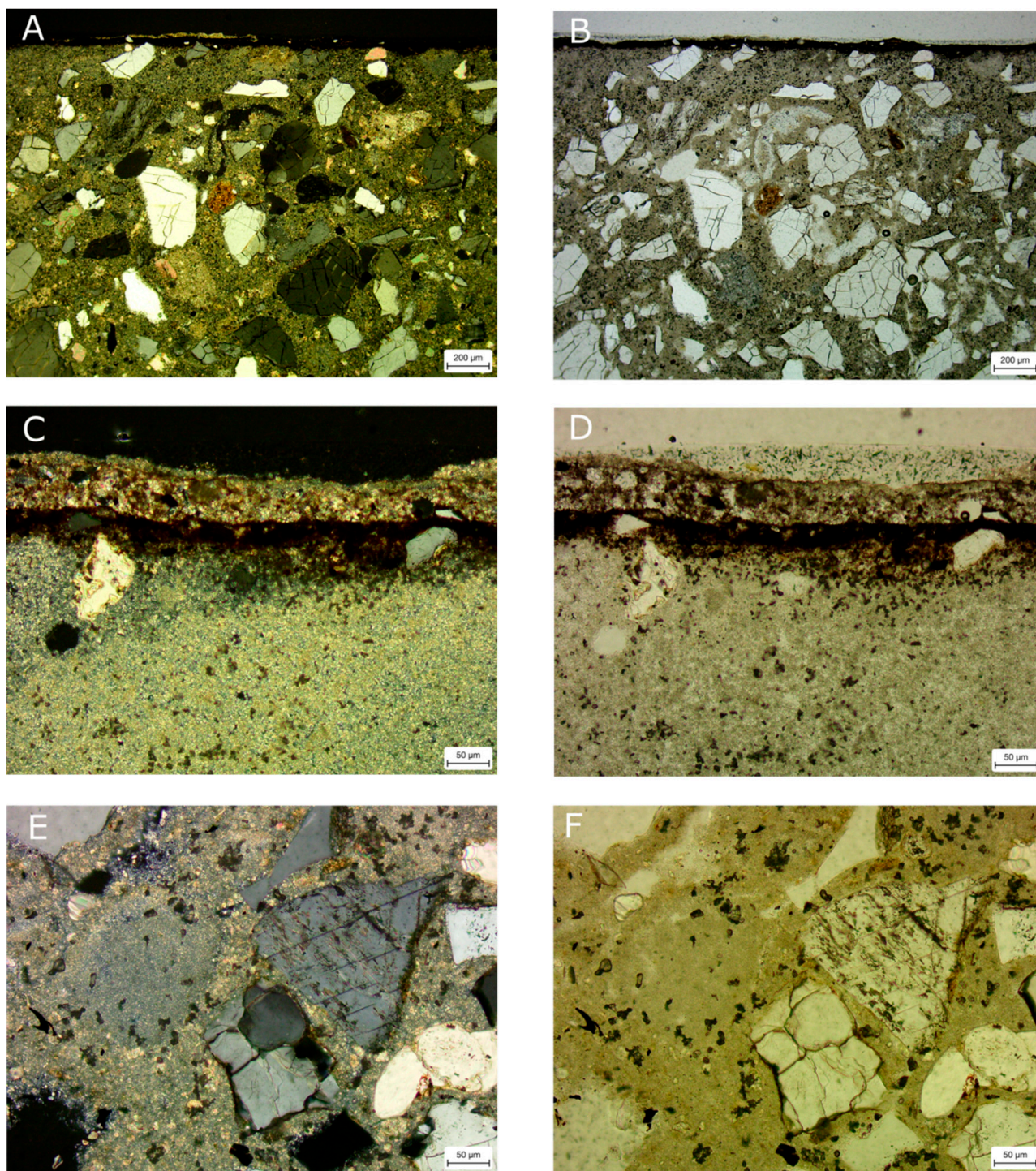
Figure 8. (**A–F**) Showing reddish aggregates (**A**); quartz grains, triangular feldspars, and plagioclase (**E,F**); and the layers checked in sample NO1 (**C,D**).

The binder is carbonated, which is mostly calcite-rich and, to a lesser extent, microsparite. Its appearance is generally homogeneous, with lumps appearing at some points (rounded lump in Figure 8E,F) and, very occasionally, nodules. The clay content is low.

The porosity is very low (less than 5%). It could be said that this microporosity is associated with the lime binder.
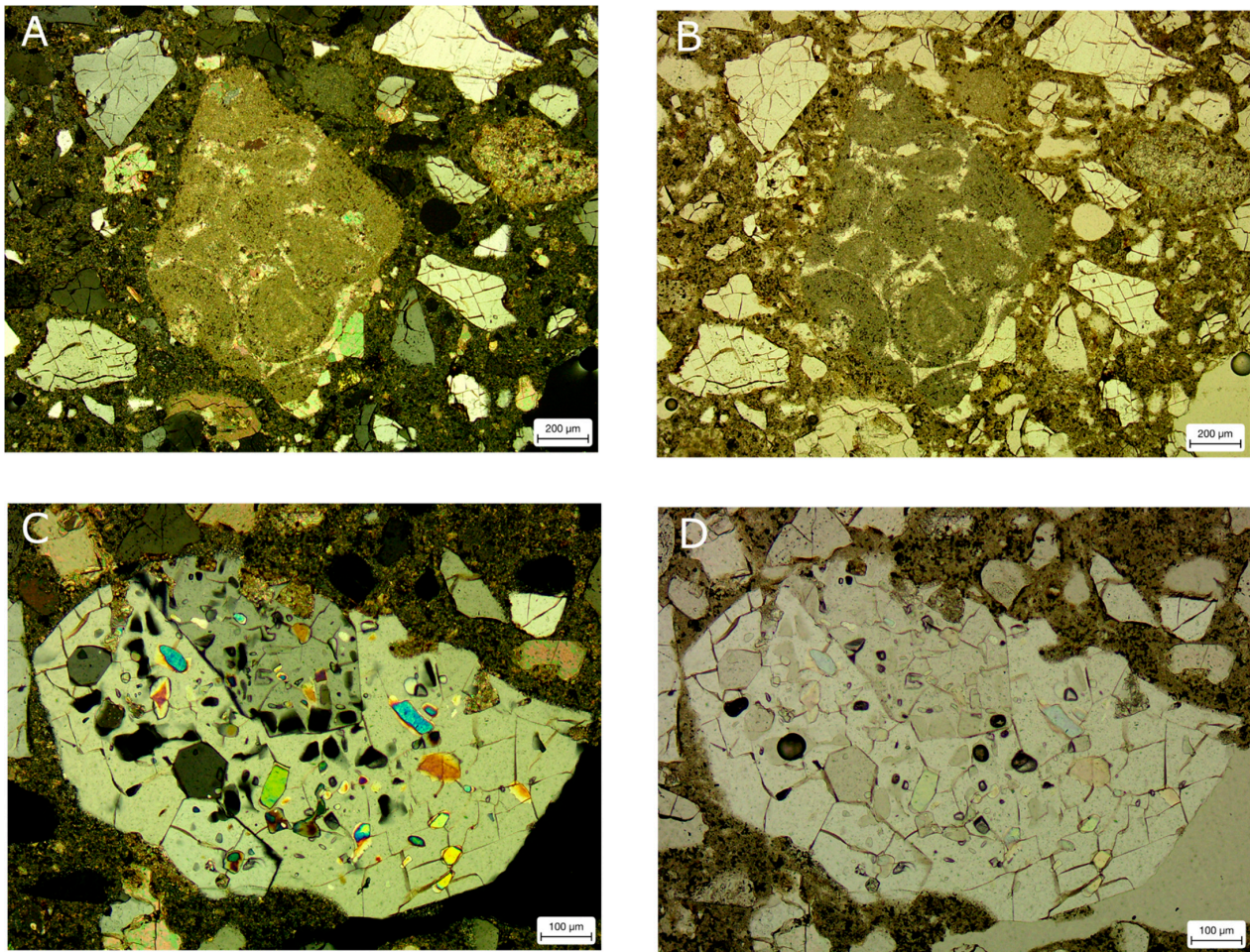
Figure 9. (**A**,**D**) Showing calcareous rock fragments in (**A**,**B**) (central view), and fractured quartz grains as the main aggregate in (**C**,**D**).

Regarding the stratigraphy of the external face of the mortar, three well-differentiated layers are observed (Figure 8C,D). The first is homogeneous, reddish, and quite opaque, with an average thickness of approximately 40 microns. The second layer is composed of a limestone binder and small quartz aggregates (approximately 20 microns) that are widely dispersed. The thickness of this layer is highly variable, ranging between 0 and 50 microns. The last and outermost layer appears to be organic in nature and has thicknesses ranging from a few microns to 50 microns, with an average thickness of 30 microns.

4.2.2. Sample NO2

The NO2 mortar presents a homogeneous mass-type texture composed mainly of lime binder, with a negligible presence of aggregates (Figure 10A–D). Aggregates are dispersed and can be seen more as binder impurities than aggregates. The grains are mica particles hundreds of microns in size (Figure 11C,D) and some scattered quartz.

The binder is carbonated, primarily calcite-rich and microsparite calcite, mainly associated with recrystallisations in the pore walls. Its appearance is homogeneous, with several lumps (rounded lump in Figure 10C,D). The clay content is low.

Interparticle porosity in the matrix is moderate (around 25%). In addition to the microporosity associated with the lime binder, there is moldic porosity (aggregates that have been degraded or dissolved) and fracture porosity.
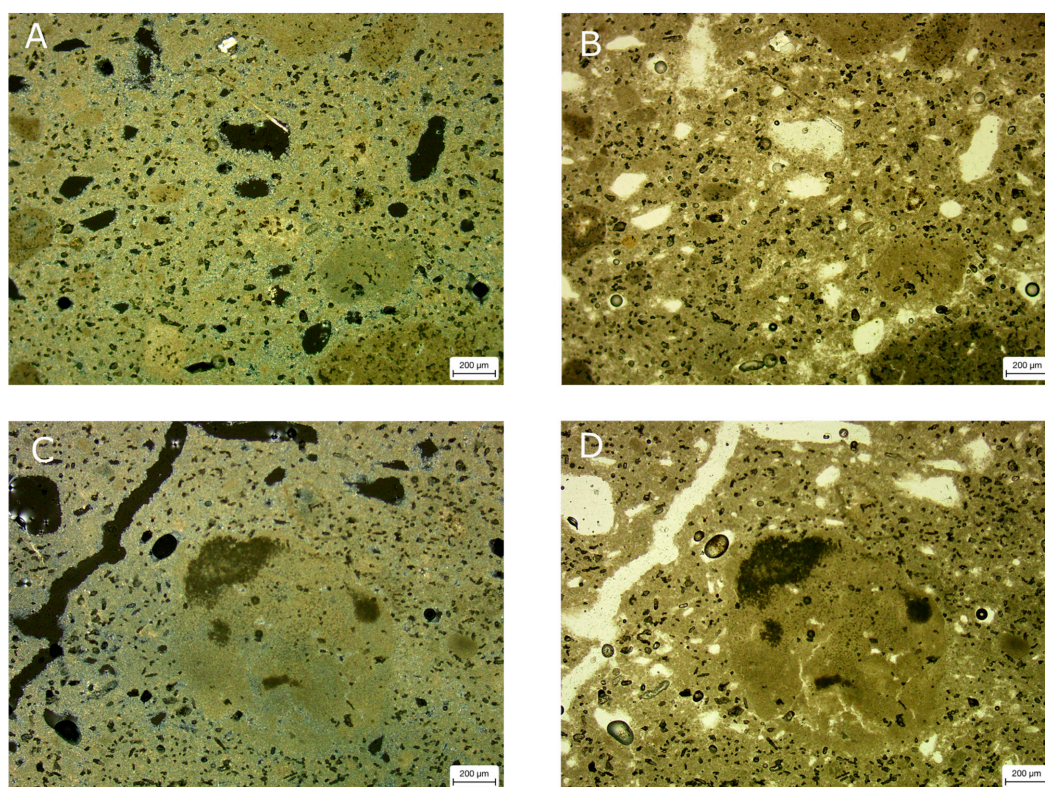
Figure 10. Photos (**A**–**D**) from sample NO2 with a low presence of aggregates. In photos (**C**,**D**), the lumps are clearly visible in the centre.
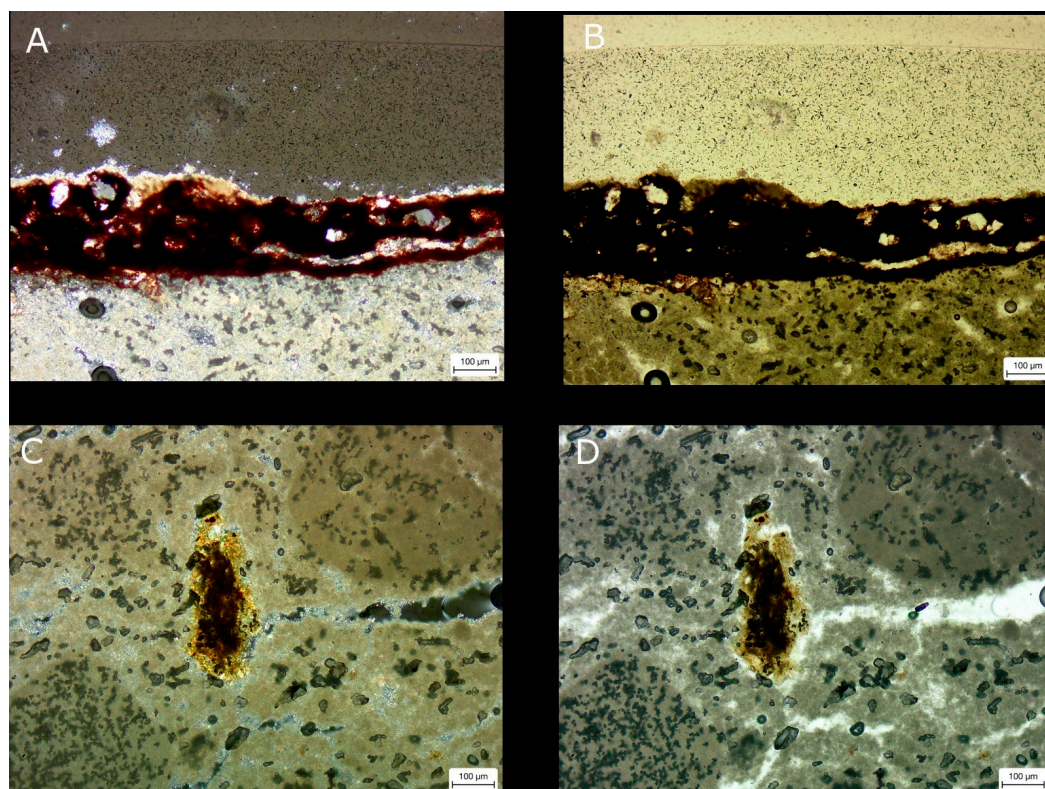

Figure 11. Photos (**A**,**B**) showing the layer with organic coating outside; photos (**C**,**D**) show micas of approximately 200 microns in size.

Regarding the stratigraphy of the mortar, it is observed that it is composed of three layers at the scale of a hand sample. Photos A and B from Figure 10 show the representative texture of the first layer. The limit where this layer meets the second one is marked by the appearance of large, elongated pores parallel to the stratification. The second layer has a similar texture to the first but with a greater presence of fractures, which increase porosity (Figure 10C,D). The last and outermost layer is composed of two clearly differentiated sublayers: the first sublayer is homogeneous, reddish and quite opaque, approximately 200 microns thick on average, with small quartz aggregates (approximately 30–40 microns) and interspersed with lumps of lime; the second sublayer appears to be organic in nature and is approximately 350 microns thick on average (photos A and B from Figure 11). The chemical analysis of these layers is currently in progress.

5. Conclusions and Discussion

The macroscopic analysis showed that the aggregates used in the renderings were made up of fine silica and limestone, with the exception of sample NO6 (baseboard of the room with the hypocaust), where the size of the aggregates means it should be classified as concrete [44–46].

Although, in all the renderings, we found calcite nodules (lumps), in the octagonal rooms (both in the finishing coat and in the fragments of mural painting), the narthex of the triclinium, and in the room to the west of the southern exedra, they were much more numerous and of larger size. This could be due to a lack of care when mixing the hydrated lime with the aggregate, despite them being very important, highly ornamented rooms. It could also be due to problems caused by bad-mixing of binder aggregates or small cavities being filled by recrystallisations of calcite from the mortar itself.

Some samples of the mortars show a more disordered, irregular distribution of the aggregate, probably due to poor mixing during preparation. They correspond to samples obtained in the rooms north of the triclinium.

All the decorative walls have either one or two layers of plastering, also called arriccio, the function of which was to level the surface of the walls. The estimated proportions were two parts of aggregate for one part of lime binder, according to the analysis of the grain-size range and the microphotographs analysed using JMicrovision software.

The use of crushed or powdered limestone as an aggregate in plastering can be corroborated by the large quantity of slightly flat, elongated calcium carbonate crystals, which differ from the more rounded crystalline structure of lime when it crystallises into calcite.

On the pictorial surface, there were visible parallel incision marks left by the "float" (a tool similar to a plastering trowel) when the surface of the plaster was smoothed while it was still wet, a feature of construction documented in other sites [47].

Regarding the data obtained through optical microscopy, all the mortars contained small amounts of magnesium-, silica-, and aluminium-rich minerals. Their presence can be attributed to the limestone (slightly loamy limestone), to the crushed and powdered limestone used as aggregate, or to both.

The plasters or intonacos of the wall paintings under study, the purpose of which is to leave a completely smooth surface ready for the application of colour, have a single preparation layer. These are mortars containing microcrystalline limestone, where it is difficult to distinguish between the binder that has crystallised in the form of calcite crystals and the aggregate composed of powdered limestone, whose calcium carbonate crystals have a grain size ranging between micrite (less than 5 microns) and microsparite (between 5 and 10 microns). In general, they are mortars rich in lime with an aggregate of limestone powder mixed in equal parts.

In view of the results obtained, some conclusions can be drawn in relation to the quantitative data obtained. Although we have not dealt with polychromes in this study, it is quite likely that the backgrounds of the wall paintings were made using the fresco

technique, while the rest of the decorative motifs, such as lines and bands, were done later using the dry technique. Altogether, this technique is known as mezzo-fresco.

The knowledge acquired in this research will allow us to undertake future restoration treatments of the remains of paintings and stucco recovered in the collapses, better respecting the geochemistry of the coatings and in more closely controlled laboratory environments. An example of this would be to use inorganic consolidators in mortars: although irreversible, they would maximise the compatibility and durability without the need to add organic resins, which sooner or later end up degrading and losing effectiveness. This is the case of lime water, silica gel, or barium hydroxide, which are currently being replaced—with very satisfactory results—by other inorganic consolidators of nanometric dimensions (around 10–20 nm), such as colloidal and aqueous dispersions of silica or nanocalcium hydroxide in alcohol dispersions, which, like lime water, are completely compatible with carbonate materials. Experimental bioconsolidation treatments could also be tested through the precipitation of calcium carbonate by the metabolic action of bacteria of the genus *Myxococcus xanthus*.

References

1. Coello, F. Caminos romanos de Cuenca. *Boletín De La Real Acad. De La Hist.* **1897**, *31*, 19–25.
2. Santa María, J. Itinerarios romanos de la provincia de Cuenca. *Boletín De La Real Acad. De La Hist.* **1897**, *31*, 5–19.
3. Larrañaga Mendia, J. *Guía de Cuenca*; Exma. Diputación: Cuenca, Ecuador, 1966.
4. Abascal Palazón, J.M. *Vías de Comunicación Romanas de la Provincia de Guadalajara*; Marqués de Santillana: Guadalajara, Mexico, 1982.
5. Palomero Plaza, S. *Las vías romanas de la provincia de Cuenca*; Diputación Provincial de Cuenca: Cuenca, Spain, 1987.
6. Valero Tévar, M.A. The mosaics of the roman *villa* of Noheda (Villar de Domingo García, Spain). *J. Roman Archaeol.* **2013**, *26*, 307–330. [CrossRef]
7. Valero Tévar, M.A. Los mosaicos de la villa romana de Noheda (Villar de Domingo García, Cuenca). In Proceedings of the XII Colloquio AIEMA, Venezia, Italy, 11–15 September 2012; pp. 439–444.
8. Valero Tévar, M.A. Anthropic dynamics and vegetation landscape in the inland area of the Iberian Peninsula: New perspectives drawn from palynological studies at the villa of Noheda (Cuenca, Spain). *Eur. J. Post-Class. Archaeol.* **2018**, *8*, 219–238.
9. Vera, D. Schiavitù rurale e colonato nell'Italia imperiale. *Sci. Dell´Anchiquità Stor. Archaeol. Antropógica* **1992**, *6–7*, 291–339.
10. Volpe, G. *Contadini, pastori e mercanti nell´Apulia tardoantica*; Munera 6; Edipuglia: Bari, Italy, 1996.
11. Sfameni, C. *Ville residenziali nell´Italia Tardoantica*; Edipuglia: Bari, Italy, 2006.
12. Chavarría Arnau, A. Villas en Hispania durante la Antigüedad tardía. In *Villas Tardoantiguas en el Mediterráneo Occidental*; Chavarría, A., Arce, J., Brogiolo, G.P., Eds.; Consejo Superior de Investigaciones Científicas, CSIC: Madrid, Spain, 2006; pp. 17–35.
13. Chavarría Arnau, A. *El final de las uillae en Hispania (Siglos IV–VIII)*; BAT 7; Brepols Publishers: Turnhout, Belgium, 2007.
14. Pensabene, P. La villa del Casale tra Tardo Antico e Medioevo alla luce dei nuovi date archaeologici: Funcioni, decorazioni e transformazioni. *Rend. Della Pontif. Accad. Romana Di Archeol.* **2011**, *83*, 141–226.

15. Hidalgo Prieto, R. ¿Fue Cercadilla una villa? El problema de la función del complejo de Cercadilla en Corduba. *Arch. Español De Arqueol.* **2014**, *87*, 217–241. [CrossRef]

16. Balmelle, C. *Les Demeures Aristocratiques d´Aquitaine*; Bordeaux/Paris, Suppl. à Aquitania, 10; Mémoires Ausonius, 5, 2001; HAL Open Science: Lyon, France, 2001.

17. Mulvin, L. *Late Roman Villas in the Danube-Balkan Region*; BAR Int. Ser. 1064; British Archaeological Report; BAR Publishing: Oxford, UK, 2002.

18. Chavarría, A. Villas in Hispania during the fourth and fifth Centuries. In *Hispania in Late Antiquity. Current Perspectives*; Bowes, K., Kulikowski, M., Eds.; Brill: Boston, MA, USA, 2005; pp. 518–555.

19. Arce, J. Villae en el paisaje rural de Hispania romana durante la Antigüedad tardía. In *Villas Tardoantiguas en el Mediterráneo Occidental*; Chavarría, A., Arce, J., Brogiolo, G.P., Eds.; Consejo Superior de Investigaciones Científicas, CSIC: Madrid, Spain, 2006; pp. 9–15.

20. Arce, J. *El Último Siglo de la España Romana, 284–409*; Alianza Editorial: Madrid, Spain, 2009.

21. Arce, J. Campos, tierras y villae en Hispania. In *Visigodos y Omeyas. El territorio*; Caballero, L., Mateos, P., Cordero, T., Eds.; Instituto Arqueológico de Mérida: Mérida, Spain, 2012; pp. 21–30.

22. García-Entero, V. *Los Balnea Domésticos-Ámbito Rural y Urbano- en la Hispania Romana*; Anejos de Archivo Español de Arqueología, XXXVII; Universidad Autónoma de Madrid: Madrid, Spain, 2005.

23. Romizzi, L. Le ville tardo-antiche in Italia. In *Villas Tardoantiguas en el Mediterráneo Occidental*; Chavarría, A., Arce, J., y Brogiolo, G.P., Eds.; Anejos del Archivo Español de Arqueología; Universidad Autónoma de Madrid: Madrid, Spain, 2006; Volume 39, pp. 37–59.

24. Hidalgo Prieto, R. El *triclinium* triconque del *palatium* de Córdoba. *An. Arqueol. Cordobesa* **1998**, *9*, 273–300. [CrossRef]

25. Dunbabin, K.M.D. *The Roman Banquet. Images of Conviviality*; Cambridge University Press: Cambrige, UK, 2003.

26. Mar, R.; y Verde, G. Las villas tardoantiguas: Cuestiones de tipología arquitectónica. In *Las villae tardorromanas en el occidente del imperio: Arquitectura y Función*; Fernández Ochoa, C., García Entero, V., y Gil Sendino, F., Eds.; Ed. Trea: Gijón, Spain, 2008; pp. 50–83.

27. Arce, J. El complejo residencial tardorromano de Cercadilla, (*Corduba*). In *Las áreas suburbanas en la ciudad histórica. Topografía, usos, función*; Anales de Arqueología Cordobesa 18; Vaquerizo, D., Ed.; Universidad de Córdoba: Córdoba, Spain, 2010; pp. 397–412.

28. Rossiter, J. Convivium and Villa in Late Antiquity. In *Dining in a Classical Context*; Slater, W.J., Ed.; University of Michigan: Ann Arbor, MI, USA, 1991; pp. 199–214.

29. Volpe, G. Stibadium e convivium in una villa tardoantica (Faragola-Ascoli-Satriano). In *Studi In Onore di Francesco Grelle*; Silvestrini, M., Spagnuolo, T., Volpe, G., Eds.; Edipuglia: Bari, Italy, 2006; pp. 319–349.

30. Valero Tévar, M.A. La iconografía del mito de Pélope e Hipodamía en la musivaria romana. Nuevas aportaciones a partir del mosaico de Noheda. *An. Arqueol. Cordobesa* **2016**, *27*, 125–160.

31. Valero Tévar, M.A. *La Persuasión de las Imágenes. Convivium y Escenografía del Poder en el Triclinium de la Villa Romana de Noheda*; Real Academia Conquense de Artes y Letras: Cuenca, Spain, 2018.

32. Hughes, J.J.; Callebaut, K. Practical sampling of historical mortars. In Proceedings of the RILEM International Workshop Historic Mortars: Characteristics and Tests; Bartos, P., Groot, C., Hughes, J.J., Eds.; RILEM: Paisley, UK, 2000; pp. 17–26.

33. Guerra García, P.; Hervás Herrera, M.A. Análisis sobre los procesos de producción de materiales constructivos en la Edad del Hierro en Thuqeibah (al-Madam, Sharjah, EAU). In *Nomina in Aqua Scripta, Homenaje a Joaquín María Córdoba Zoilo*; Domínguez Monedero, A.J., del Cerro Linares, D., Villalba Ruiz de Toledo, F.J., Borrego Gallardo, F.L., Eds.; UAM Ediciones: Madrid, Spain, 2021; pp. 211–232.

34. Adriano, P.; Santos Silva, A. *Caracterização de Argamassas Antigas da Igreja de Santa Maria de Évora- Sé Catedral de Évora*; Relatório LNEC, 59/06; NMM: Lisbon, Portugal, 2006; 86p.

35. Antonelli, F.; Lazzarini, L.; Cancelliere, S.; Dessandier, D. Volubilis (Meknes, Morocco): Archaeometric Study of the White and Coloured Marbles Imported in the Roman Age. *J. Cult. Herit.* **2009**, *10*, 116–123. [CrossRef]

36. Sitzia, F.; Beltrame, M.; Lisci, C.; Mirão, J. Micro Destructive Analysis for the Characterization of Ancient Mortars: A Case Study from the Little Roman Bath of Nora (Sardinia, Italy). *Heritage* **2021**, *4*, 2544–2562. [CrossRef]

37. Grillo, V.; Rossi, F. STEM_CELL: A Software Tool for Electron Microscopy. Analysis of Crystalline Materials. *Ultramicroscopy* **2013**, *125*, 112–129. [CrossRef] [PubMed]

38. Larrea, M.L.; Castro, S.M.; Bjerg, E.A. A Software Solution for Point Counting. Petrographic Thin Section Analysis as a Case Study. *Arab. J. Geosci.* **2014**, *7*, 2981–2989. [CrossRef]

39. Prendes Rubiera, N. Tratamiento digital de imágenes como herramienta de evaluación y análisis en la restauración. *ReCoPaR* **2006**, *1*, 1886–2497.

40. Ingham, J. *Geomaterials Under the Microscope*; CRC Press: Manson, IA, USA, 2010.

41. Pecchioni, E.; Fratini, F.; Cantisani, E. *Atlante delle Malte Antiche in Sezione Sottile al Microscopio Ottico*; Nardini Editore: Florence, Italy, 2014.

42. Solà-Morales, P.; Puche, J.M.; Macias, J.M.; Toldrà, J. Ensayos de nuevos análisis óptico-visuales para el análisis de estructuras arquitectónicas-patrimoniales. El uso de la reflectancia láser. In *Modelos Constructivos y Urbanísticos de la Arquitectura de Hispania Definición, Evolución y Difusión del Periodo Romano a la Antigüedad Tardía*; Roldan, L., Macias, J.M., Pizzo, A., Rodriguez, O., Eds.; Institut Català d'Arqueologia Clàssica: Tarragona, Spain, 2017; pp. 77–89.

43. Guerra García, P. The Study of the Late Antique Structures of Egitania by Means of its Mortars. In *De Ciuitas Igaeditanorum a Laŷdāniyya. Paisajes Urbanos de Idanha-a-Velha (Portugal) en Épocas Tardoantigua y Medieval*; Morín de Pablos, J., Sánchez Ramos, I., Eds.; BAR Publishing: Oxford, UK, 2019; pp. 135–150.

44. Angelici, E.; Grassini, S.; Fulginiti, D.; Parvis, M.; Segimiro, A. *Compatibilità and Efficency of Restoration Products for Artefacts in Neapolitan Yellow Tuff, Scienza e Beni Culturali*; Università degli Studi di Napoli: Bressanone, Italy, 2013.

45. Borsoi, G.; Veiga, R.; Santos Silva, A. Effect of nanostructured lime-based and silica-based products on the consolidation of historical renders. In Proceedings of the 3rd Historic Mortars Conference, Glasgow, UK, 11–14 September 2013; UWS University: Glasgow, UK, 2013.

46. Licchelli, M.; Weththimuni, M.; Zanchi, C. Nanoparticles for the Consolidation of Lecce Stone. In Proceedings of the Atti del XXIV Congresso Nazionale della Società Chimica Italiana, Lecce, Italy, 11–16 September 2011; Università di Parma: Parma, Italy, 2013.

47. *BS En 12620*; Aggregates for Concretes. British Standards Institution: London, UK, 2002.